Global patterns of extreme temperature teleconnections using climate network analysis

Yuhao Feng, Jun Meng, Jingfang Fan

Originally published as
Feng, Y., Meng, J., Fan, J. (2025): Global patterns of extreme temperature teleconnections using climate network analysis . - Chaos, 35, 6, 061106.
https://doi.org/10.1063/5.0276151

RESEARCH ARTICLE | JUNE 17 2025

Global patterns of extreme temperature teleconnections using climate network analysis

Yuhao Feng ; Jun Meng ; Jingfang Fan

Chaos 35, 061106 (2025)
https://doi.org/10.1063/5.0276151

Global patterns of extreme temperature teleconnections using climate network analysis

Cite as: Chaos 35, 061106 (2025); doi: 10.1063/5.0276151
Submitted: 16 April 2025 · Accepted: 15 May 2025 ·
Published Online: 17 June 2025

Yuhao Feng,[1] Jun Meng,[2,a)] and Jingfang Fan[3,4,b)]

AFFILIATIONS

[1]School of Science, Beijing University of Posts and Telecommunications, Beijing 100876, China
[2]State Key Laboratory of Earth System Numerical Modeling and Application, Institute of Atmospheric Physics, Chinese Academy of Sciences, Beijing 100029, China
[3]School of Systems Science/Institute of Nonequilibrium Systems, Beijing Normal University, Beijing 100875, China
[4]Potsdam Institute for Climate Impact Research, Potsdam 14412, Germany

[a)]**Electronic mail:** mengjun@mails.iap.ac.cn
[b)]**Author to whom correspondence should be addressed:** jingfang@bnu.edu.cn

ABSTRACT

Extreme weather events, rare yet profoundly impactful, are often accompanied by severe conditions. Increasing global temperatures are poised to exacerbate these events, resulting in greater human casualties, economic losses, and ecological destruction. Complex global climate interactions, known as teleconnections, can lead to widespread repercussions triggered by localized extreme weather. Understanding these teleconnection patterns is crucial for weather forecasting, enhancing safety, and advancing climate science. Here, we employ climate network analysis to uncover teleconnection patterns associated with extreme day-to-day temperature differences, including both extreme warming and cooling events occurring on a daily basis. Our study results demonstrate that the distances of significant teleconnections initially conform to a power-law decay, signifying a decline in connectivity with distance. However, this power-law decay tendency breaks beyond a certain threshold distance, suggesting the existence of long-distance connections. Additionally, we uncover a greater prevalence of long-distance connectivity among extreme cooling events compared to extreme warming events. The global pattern of teleconnections is, in part, likely driven by the mechanism of Rossby waves, which serve as a rapid conduit for inducing correlated fluctuations in both pressure and temperature. These results enhance our understanding of the multiscale nature of climate teleconnections and hold significant implications for improving weather forecasting and assessing climate risks in a warming world.

Extreme heat and cold can occur synchronously at distant locations, yet the mechanisms linking these events across the globe remain incompletely understood. Our research shows that cold spells and heatwaves are often linked over long distances—especially cold events—which can be traced through patterns in daily temperature extremes. These links weaken with distance up to a point, but then surprisingly reappear across continents, largely driven by powerful atmospheric waves. This discovery helps us better understand how extreme weather propagates and could improve forecasts as the climate continues to change.

I. INTRODUCTION

Extreme weather events, invariably accompanied by severe weather conditions, are extraordinary and infrequent occurrences characterized by their low likelihood of happening but with profound and devastating consequences for human lives and society. Current observational evidence and climate model projections consistently indicate that rising global temperatures will intensify the frequency and severity of extreme weather events across the globe,[1–4] leading to a heightened magnitude of human casualties, extensive damage, increased economic burdens, and the destruction of ecosystems. Complex interactions and teleconnections within the global climate system pose potential threats to the world.[5,6] Weather conditions, especially extreme events in one location, can have far-reaching effects, triggering a chain reaction of consequences on a global scale.[7] Hence, unraveling the teleconnection patterns of extreme weather events worldwide holds significant importance for weather forecasting, enhancing human safety, and gaining a deeper understanding of climate mechanisms,[8,9] particularly in the context of a warming global climate.[10]

The Earth's climate system consists of highly interconnected, nonlinear subsystems governed by intricate interactions and feedback mechanisms that span diverse spatial and temporal scales.[11] Employing a complex network approach to model the climate system offers valuable insights into its dynamic and interconnected behavior. Climate Network (CN) analysis, grounded in complex network theory, represents the climate system as a network in which nodes correspond to geographical locations and links encode statistical relationships—such as correlations or synchronizations—between climate variables at different regions.[8,9] Over the past decade, CNs have proven to be a versatile and powerful framework for analyzing climatic time series. For instance, Pearson correlation-based networks have yielded significant results in characterizing El Niño–Southern Oscillation.[12–14] Similarly, event synchronization networks have been successfully applied to investigate the spatiotemporal structure of extreme-rainfall events.[6,15,16] Furthermore, mutual information-based networks have effectively captured the westward propagation of sea surface temperature (SST) anomalies associated with the Atlantic Multidecadal Oscillation, as demonstrated by Feng and Dijkstra.[17]

In this study, we employ the event synchronization CN framework[6] to investigate the spatial distribution of interactions among extreme weather events. We concentrated on abrupt extreme temperature changes—specifically, daily temperature differences (current day minus previous day), calculated from temperatures with the mean seasonal cycle removed, that exceed the 97.5th percentile (extreme warming) or fall below the 2.5th percentile (extreme cooling) of each grid cell's historical distribution. Unlike conventional definitions of heatwaves or cold spells that emphasize sustained deviations from climatological means, our method captures extreme events based on abrupt, day-to-day temperature differences—thereby targeting short-term, high-impact fluctuations more relevant to atmospheric teleconnection dynamics. These extreme events are of particular interest due to their disruptive impacts on weather forecast accuracy and daily human activities, posing considerable risks to human safety and well-being. We find that extreme weather events occur less frequently over continents than over oceans, primarily due to differences in thermal dynamics. On a global scale, extreme events exhibit a relatively uniform distribution along longitudes but display distinct patterns along latitudes, reflecting the influential role of the jet stream in modulating weather phenomena such as storms. Within the framework of CN analysis, we identify both source regions that can significantly influence weather conditions elsewhere and sink regions that are particularly vulnerable to such external disruptions. Notably, our analysis reveals robust teleconnections between spatially distant extreme events, suggesting the potential for cascading effects within the climate system—potentially triggered through synchronization mechanisms. These findings emphasize the critical need to understand the complex interdependencies of the Earth's climate system to enhance the accuracy of climate modeling and forecasting.

II. RESULTS

We utilize daily air temperature data at the 1000 hPa pressure level from ERA5 reanalysis,[18] with a spatial resolution of $2.5^\circ \times 2.5^\circ$, encompassing 10 512 grid points globally. Due to the Earth's oblate spheroid shape, the actual ground distance represented by a given longitudinal interval decreases toward higher latitudes. To achieve a more uniform spatial sampling, we follow the method described in Sec. IV B, selecting 6570 nodes from the original set of 10 512 to ensure approximately equal-area coverage across the globe.[12] For each node (i.e., latitude–longitude grid point), we analyze daily temperature records from 1 January 1979 to 31 December 2021, after removing the mean seasonal cycle and normalizing by the corresponding seasonal standard deviation.

To identify extreme events, we define node-specific thresholds using the 97.5th percentile for positive (extremely warm) events [Fig. 1(a)] and the 2.5th percentile for negative (extremely cold) events [Fig. 1(b)]. Sequences of consecutive days exceeding these upper or lower thresholds are treated as a single extreme event. A comprehensive description of the detection criteria is provided in Sec. IV A. As shown in Figs. 1(a) and 1(b), the upper and lower temperature thresholds are less pronounced near the equator than at higher latitudes, especially over oceans. This indicates lower temperature variability at lower latitudes, where equatorial temperatures remain nearly constant year-round, varying by only a few degrees.[19] Additionally, Figs. 1(c) and 1(d) reveal that regions with fewer detected extreme events are predominantly continental. However, this does not imply that extreme weather is less frequent over land than over oceans. Rather, the reduced event count on land is primarily due to event clustering,[20] where sequences of consecutive days with abrupt extreme temperature changes are aggregated as a single event. This contrast arises from the distinct thermal dynamics of land and ocean surfaces. Oceans, with their higher heat capacity, absorb and retain heat over extended periods, resulting in more temporally dispersed extreme events. In contrast, land surfaces, which heat and cool more rapidly due to lower heat capacity, tend to experience more frequent and tightly grouped extreme events. Furthermore, the observed lower frequency of extreme events in mid-latitudes suggests that the jet stream plays a critical role in organizing storm systems, thereby promoting the clustering of temperature anomalies in these regions.[21] Although a uniform percentile-based definition is used across all regions, differences in thermal inertia between the land and ocean produce natural disparities in the event frequency. These do not invalidate the synchronization-based network results but should be considered when interpreting spatial asymmetries in connectivity.

We quantify connections among extreme events using the event synchronization CN method (see Secs. IV B and IV C). Network links are established between nodes when synchronization values are significant ($P < 0.005$; see Sec. IV E). Each node's degree, defined as the number of significant links, reflects its interaction with the global climate system—higher degrees indicate stronger connectivity, while lower degrees suggest isolation.

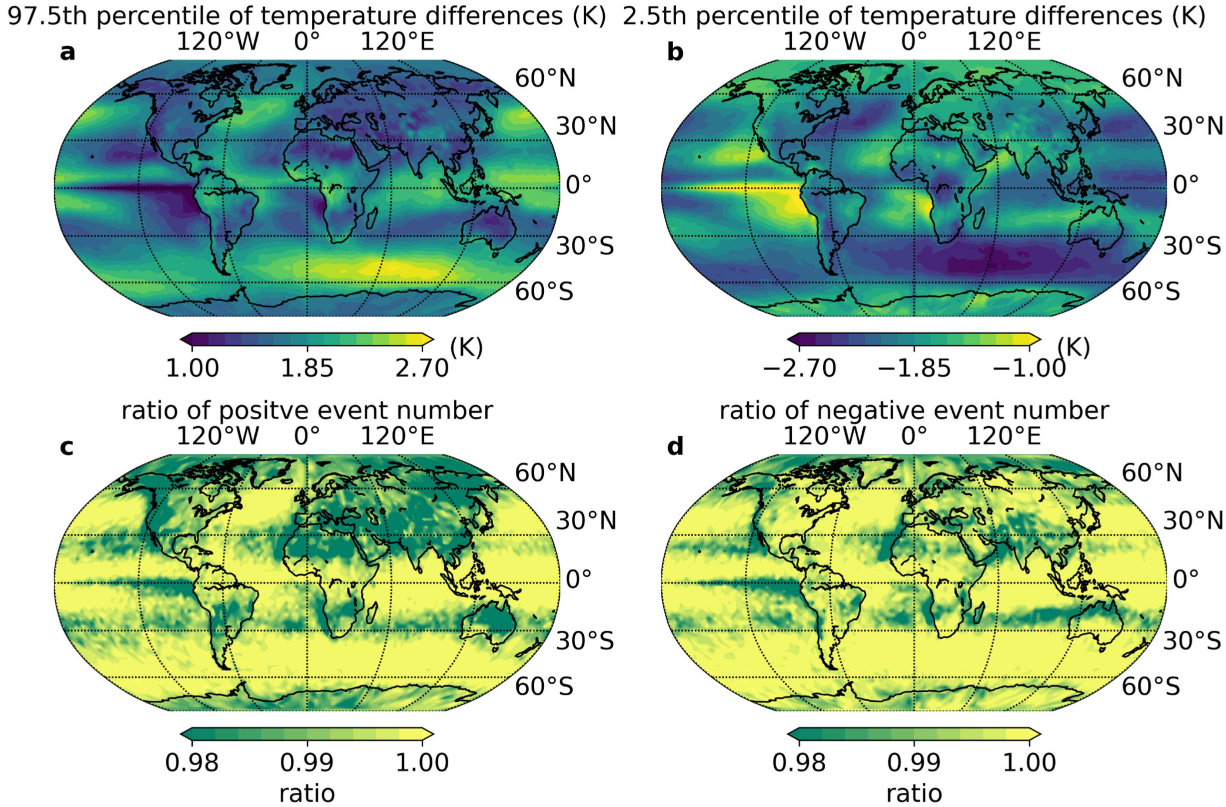

FIG. 1. Spatial patterns based on day-to-day air temperature differences by the threshold of 97.5% (pst) and 2.5% (ngt) changes. (a) Values of the 97.5th percentile of day-to-day air temperature differences from 1979 to 2021, computed individually for each of the 6570 timeseries obtained from the $2.5^\circ \times 2.5^\circ$ grid cells of the ERA5 data set. (b) As in (a), but under the 2.5th percentile of day-to-day air temperature differences. As the difference approaches zero, it indicates a higher level of temperature stability within the respective region. (c) Ratio of extreme warming events [exceeding the 97.5th percentile of day-to-day air temperature differences, as defined in (a)] to the theoretical maximum number of such events ($\lceil 15\,694 \times 2.5\% \rceil = 393$). Consecutive days above the threshold are counted as a single event. (d) As in (c), but for extreme cooling events (below the 2.5th percentile of day-to-day air temperature differences).

Using this approach, we constructed three CNs: the positive-to-positive (PP) network, based on synchronized positive events; the negative-to-negative (NN) network, based on synchronized negative events; and the positive-to-negative (PN or NP) network, based on synchronized positive (negative) and negative (positive) events.

Our findings, presented in Figs. 2(a)–2(c), reveal a striking pattern: although extreme events are most frequent near the equator [see Figs. 1(c) and 1(d)], these equatorial nodes exhibit near-zero degrees—indicating limited connectivity with the broader CN. In contrast, polar and mid-latitude regions—particularly continental areas such as the Amazon, Southeast China, eastern Australia, and Northern Africa—demonstrate significantly higher node degrees, suggesting stronger interactions within the climate system. Notably, negative extreme events show greater overall connectivity: the NN and PN networks display markedly higher node degrees than the PP network [Figs. 2(b), 2(c) vs 2(a)]. These observations raise two critical questions: (1) What are the spatial origins of the significant links associated with high-degree nodes, and how do they relate to regional influence? (2) What is the directionality of these links—do they signify a node's role as a source of disruption (influential) or as a recipient (vulnerable)?

To address the first question, we analyze the Probability Density Function (PDF) of distances for significant links using a power-law relationship, expressed as $p(d) \propto d^{-\alpha}$, where d denotes the great-circle distance between nodes (in km), $p(d)$ is the probability density of links at distance d, and α is the power-law scaling exponent. Figures 2(d)–2(f) reveal a multiscale teleconnection structure. At local spatial scales (1000–3000 km), all three network types (PP, NN, and PN) show a power-law decay, reflecting a rapid drop in synchronization likelihood with distance in link probability, indicating a rapid decline in synchronization likelihood with increasing distance. However, beyond approximately 4000 km, the distributions deviate from this scaling behavior, showing enhanced tails or secondary peaks. The distance distribution of significant long-range connections, as estimated via kernel density estimation [KDE, shown as the black solid line in Figs. 2(d)–2(f)], deviates markedly from the short-range power-law decay. This distribution

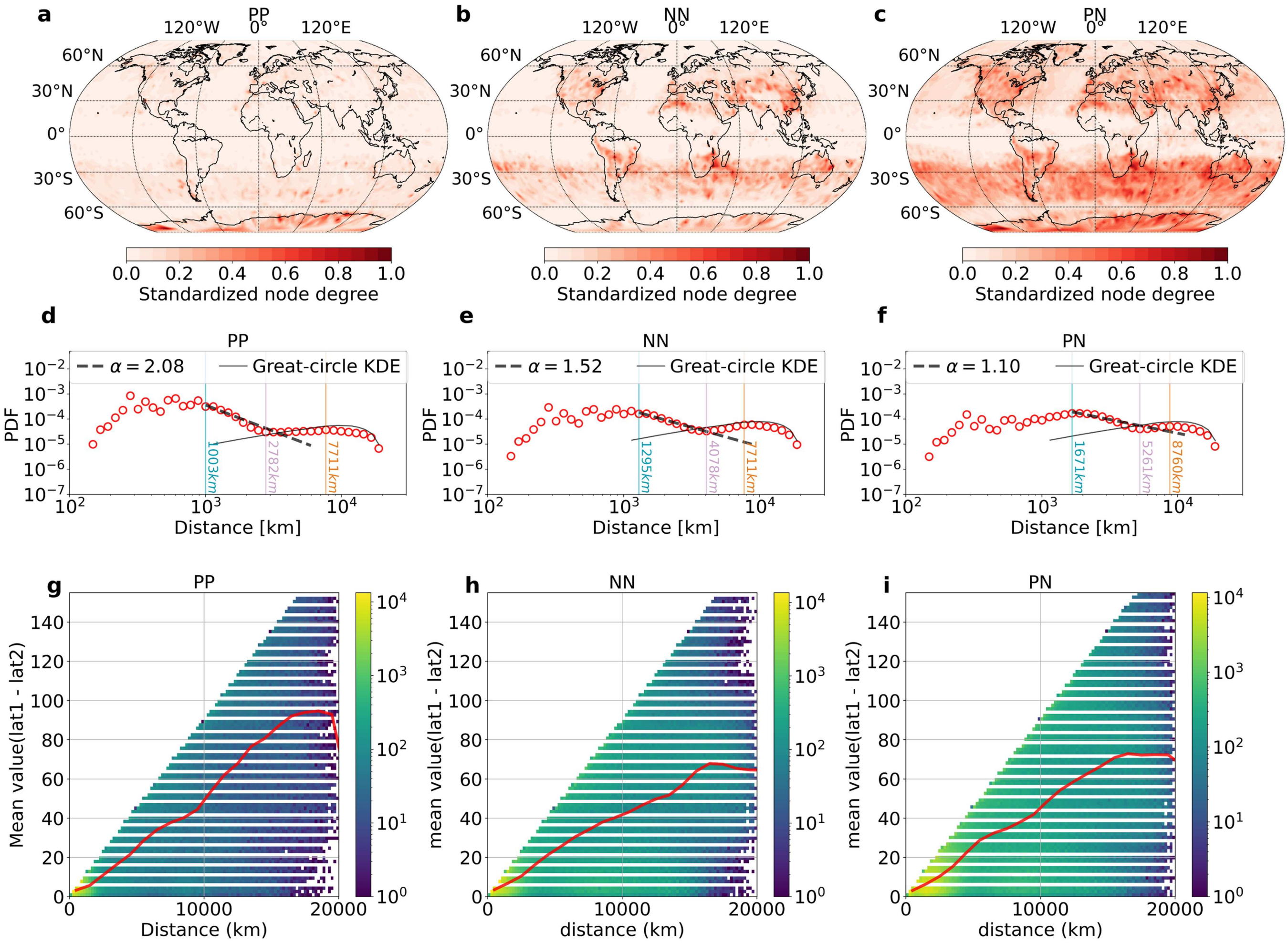

FIG. 2. Characteristics of climate networks based on extreme-event synchronizations. (a)–(c) Spatial distribution of node degrees for the positive–positive (PP), negative–negative (NN), and positive–negative (PN) climate networks, respectively. Colorbars are labeled "standardized node degree." (d)–(f) Probability density functions (PDFs) of link distances, defined as the great-circle distance between pairs of nodes connected by significant links. Power-law fits are shown as dashed black lines over the relevant range, while the kernel density estimate (KDE) of the distribution of all possible great-circle distances is depicted as a black solid line. (g)–(i) Latitude difference analysis of synchronized node pairs. Each panel shows the absolute difference in the latitude (in degrees) between linked nodes. Red lines indicate the mean latitude difference within each bin.

conforms to the natural great-circle distance distribution among grid cells. Such conformity indicates that long-range connections are principally governed by Rossby waves, whose propagation approximates great-circle paths—the shortest routes on the Earth's spherical surface. Therefore, the observed long-distance distribution is determined by planetary-scale geometric constraints rather than a random power-law decay, which provides a mechanistic rationale for the deviation from local scaling behavior. These long-range teleconnections correspond to "dragon kings"[22,23]—extreme, statistically anomalous events that stand out from the expected short-range scaling law. This finding suggests that remote synchronization between extreme events arises from underlying processes that cannot be inferred from local dynamics alone, highlighting the presence of emergent global-scale organizing mechanisms in the climate system.[24]

Additionally, we find that extreme cooling events exhibit a higher prevalence of long-distance teleconnections compared to extreme warming events. This is evident in the NN network, which shows a pronounced secondary peak in the link distance distribution beyond 4000 km [Fig. 2(e)]—a feature largely absent in the PP network [Fig. 2(d)]. Using 4632 km (the power-law decay breakpoint) as a threshold, 60.7% of NN network links are long-range, compared to 40.2% in the PP network—a difference of 20.4%. When using 7711 km (near the upper bound of Rossby wave scales), the difference remains robust: 48.1% for NN vs 30.8% for PP (difference = 17.3%). These results confirm that extreme cooling events are more frequently associated with robust long-distance synchronization, whether defined by the scale break in the distance distribution or known atmospheric waveguide characteristics.

High-degree nodes are predominantly clustered in mid-latitude and polar regions [Figs. 2(a)–2(e)], aligning with jet stream pathways and the propagation of Rossby waves, which facilitate the long-range transport of atmospheric perturbations across thousands of kilometers. For instance, the NN network's secondary peak at 6000–8000 km [Fig. 2(e)] matches typical Rossby wave wavelengths, implicating them in long-distance cold-air outbreaks and synoptic disturbances.[6,25] This interplay likely drives synchronization across vast distances, such as linking polar cold outbreaks with downstream cooling. Furthermore, Figs. 2(g)–2(i) reveal that long-distance synchronization often involves cross-latitude and even cross-hemispheric connectivity, which is consistent with the influence of Rossby waves and jet stream dynamics in facilitating energy transport across climatic zones. Overall, the multiscale patterns in Fig. 2 reflect dual mechanisms: local high-frequency coupling (short-range power-law decay) and remote wave-driven propagation (long-range Rossby wave effects).

To address the second question, we incorporate directional information into the original CNs by determining the direction of each link based on time lags of synchronized events between nodes (see Sec. IV D). We define a node's out-degree as the number of outgoing links and its in-degree as the number of incoming links (see Sec. IV F). The out-degree reflects the node's influence on the global climate system, while the in-degree indicates its susceptibility to external impacts. We further adopt the concept of divergence, calculated as the out-degree minus the in-degree. A high positive divergence signifies a node's strong influence on the climate system, whereas a high negative divergence indicates greater vulnerability. Network divergence enables the identification of influential or vulnerable regions within the system.

Our analysis (Fig. 3) reveals a pronounced concentration of high divergence in the southern mid-to-high latitudes (20 °S–60 °S), indicating that this region functions predominantly as a net source of extreme temperature events—actively propagating signals rather than passively receiving them. For the PP network [Fig. 3(a)], when Southern Hemisphere westerlies shift northward or intensify, enhanced warm air advection strengthens heat exchange between mid-latitude warm oceanic regions—especially near the northern boundary of the Southern Ocean—and the overlying atmosphere. This process, coupled with planetary-scale or regional circulation anomalies, can trigger extreme warming events and propagate "warming signals" downstream.[26,27]

In the NN network [Fig. 3(b)], this spatial structure aligns with known impacts of the negative phase of the Southern Annular Mode (SAM), which tends to displace westerlies northward and can facilitate cold-air advection from polar regions. While our network patterns are consistent with these dynamics, we do not perform explicit SAM index correlation or circulation diagnostics, so this interpretation remains a hypothesis supported by the prior literature.

For the PN network [Fig. 3(c)], phase shifts in background flow—such as changes in westerly speed or intensity—modify the propagation characteristics of Rossby waves. These alterations induce abrupt transitions between warming and cooling events across different longitudes within the same latitude band, reflecting dynamic interactions between opposing extreme events.[28,29]

Moreover, Fig. 3 demonstrates that the importance of high-divergence regions extends beyond their immediate influence: we observe a notable spatial overlap between regions exhibiting high-divergence values (± 0.6 to ± 0.8) and key climate tipping elements, including the Antarctic Ice Sheet, North American and Eurasian boreal forests, and the Amazon rainforest.[30,31] This spatial coincidence suggests that state transitions in these regions—particularly the onset of tipping points—may not only cause localized disruptions but also amplify and trigger extreme events that propagate globally through the synchronization network of extremes. Motivated by this insight and the consistently high-divergence values observed in Fig. 2 (ranging from 0.6 to 1), we focus on the Amazon rainforest as a case study to further investigate the teleconnection structure associated with extreme cold events (see Fig. 4).

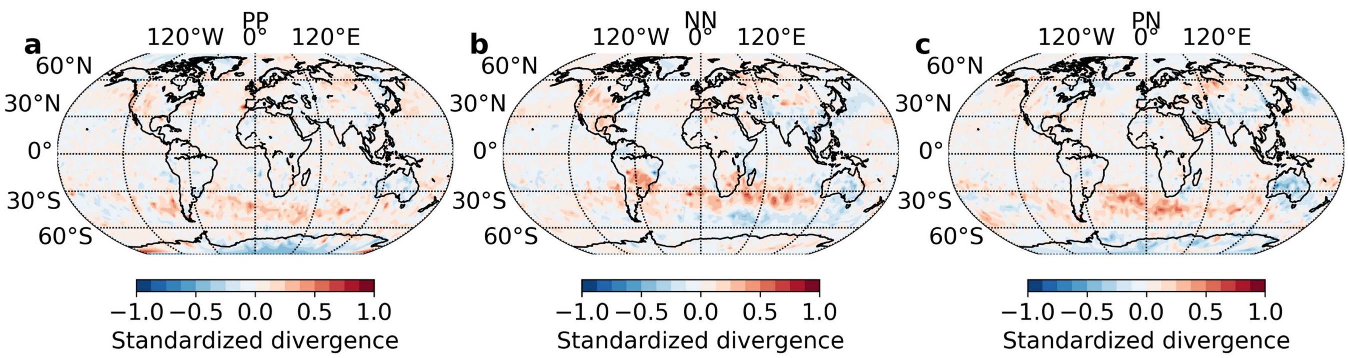

FIG. 3. Some characteristics about the directed climate network of extreme-event synchronizations. (a)–(c) Spatial distribution of divergence for positive-to-positive (PP), negative-to-negative (NN), and positive-to-negative (PN) climate networks, respectively. Divergence, defined as the difference between out-degree and in-degree for each grid cell, is standardized by dividing by the maximum absolute divergence value to enable meaningful comparisons across networks. Color scales range from −1 to 1, with positive values (red) indicating a node's influence and negative values (blue) indicating vulnerability.

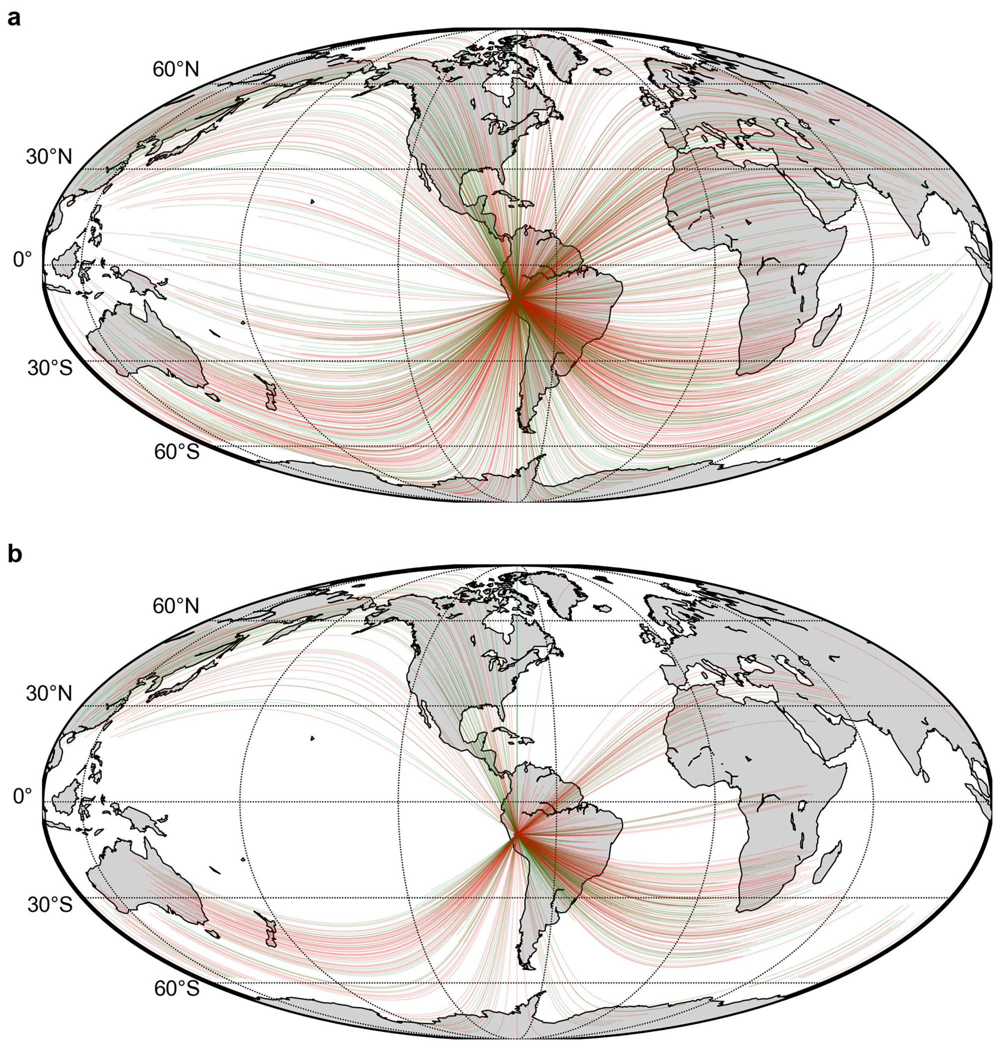

FIG. 4. Out-links and in-links of negative-to-negative (NN) climate networks in the Amazon (red lines denote the out-edges, and green lines denote the in-edges). (a) Uncorrected out-links and in-links network. (b) Corrected out-links and in-links network.

Before proceeding, we address a fundamental statistical challenge inherent in all data-driven correlation analyses, particularly when constructing networks based on statistical similarity. These methods are highly susceptible to multiple comparison bias. In our case, each time series was compared with 6569 others, yielding over 10^8 pairwise comparisons. Consequently, the resulting network may contain spurious links that arise purely by chance, rather than reflecting genuine physical connections. This issue is particularly relevant for the spatial distribution of network connections linked to the Amazon rainforest [see Fig. 4(a)]. To mitigate this, we apply a spatial density estimation method (see Sec. IV G) to identify statistically significant ($P < 0.001$) spatial link bundles. This procedure effectively accounts for multiple testing within the spatially embedded functional network. All links outside these statistically validated bundles are removed, allowing us to isolate physically meaningful couplings with greater confidence.

After correction, the refined data reveal a robust pattern of stable link bundles between the Amazon rainforest and distant regions, including Europe, eastern Australia, tropical Africa, and the mid-latitudes of the Southern Hemisphere. As shown in Fig. 4(b), these connections, depicted as red (out-degree) and green (in-degree) edges during extreme cold events in the Amazon, capture reciprocal teleconnections across specific spatial and temporal scales. This distinctive network structure provides direct empirical evidence for examining how large-scale atmospheric waves mediate the propagation of regional extreme climate events. Strikingly, this edge pattern aligns well with known atmospheric teleconnection pathways governed by Rossby waves. As dominant features of mid-to-high latitude atmospheric dynamics, Rossby waves exhibit characteristic wavelength ranges that closely match the spatial distances of these links. This suggests that during extreme cold events in the Amazon, cold-air anomalies may be transmitted to Europe, eastern Australia, and tropical Africa via Rossby wave trains. Simultaneously, the Amazon also receives feedback from these regions, forming a complex bidirectional interaction. Thus, the Amazon functions as both a *driver* and *responder* of influence within the global extreme-event network, underscoring its pivotal and dynamic role in the Earth's climate system.[32]

III. DISCUSSIONS

In this study, we have developed a comprehensive CN approach to unravel the teleconnection patterns of extreme temperature events. By leveraging event synchronization techniques, our work captures both local interactions and remote, long-range connections that are predominantly mediated by atmospheric wave dynamics.

One of the main findings is the power-law decay in the probability density of link distances at scales up to approximately 4000 km. This decay indicates that the likelihood of two regions experiencing synchronized extreme events decreases rapidly with distance. However, the observed deviation beyond this threshold points to the existence of a secondary mechanism—likely associated with the propagation of Rossby waves—which facilitates robust teleconnections over intercontinental distances. The emergence of "dragon king" type anomalies in the link distance distribution underscores that remote regions can become unexpectedly connected, a phenomenon that has significant implications for our understanding of climate variability.

Furthermore, our directed network analysis sheds light on the roles of individual nodes within the global climate system. Regions exhibiting high positive divergence are identified as key drivers capable of influencing distant areas through rapid atmospheric processes. In contrast, high positive divergence nodes (e.g., mid-latitude oceans) act as sources of extreme-event propagation, while high negative divergence areas (e.g., polar regions) are vulnerable to external perturbations. The overlap between these high-divergence zones and climate tipping elements (e.g., Amazon rainforest) is a notable discovery, indicating a strong correlation and raising the hypothesis that disturbances in these "conduit regions" might trigger cascading effects via atmospheric pathways. For example, extreme cooling in the Amazon was linked to synchronized events in Europe and Australia, mediated by Rossby wave trains, highlighting the potential for remote tipping element interactions. Note that while these examples support a Rossby wave interpretation, further generalization would require systematic dynamical diagnostics (e.g., wave activity flux, phase speed, or Hovmöller diagrams) across the entire data set.

As a complement to the present global-scale analysis, future research may delve into surface-type-specific teleconnection patterns by explicitly categorizing grid cells into the land and ocean. This could enable a more nuanced understanding of how extreme events synchronize over different surface types—for example, whether oceans, with higher heat capacity, exhibit stronger long-range coherence than continents, where land heterogeneity may fragment such connections. This approach could help clarify whether the robust long-distance links identified in this study [e.g., Rossby wave-mediated structures in Figs. 2(d)–2(f) are modulated by surface properties or primarily governed by atmospheric wave dynamics].

Overall, our results emphasize the dual role of local thermodynamic processes and large-scale atmospheric dynamics in governing extreme temperature teleconnections. As global warming intensifies, the frequency and impact of these events are likely to increase, making it imperative to incorporate such network-based insights into future climate forecasting and risk management strategies. By bridging the gap between short-term variability and long-term climate change, our study provides a more nuanced understanding of the interconnected nature of extreme weather phenomena and highlights the urgent need to monitor and mitigate potential cascading effects in a warming world.

IV. DATA AND METHODS

All analyses span 1 January 1979 to 31 December 2021, leveraging daily air temperature data at the 1000 hPa pressure level from the ERA5 reanalysis data set.[18]

A. Data

The data utilized in this study were extracted from the ERA5 reanalysis data sets, available through the European Centre for Medium-Range Weather Forecasts (ECMWF) website.[18] The data exhibit a spatial resolution of 2.5° in both the zonal (latitude) and meridional (longitude) directions. This study predominantly employs the air temperature data at the 1000 hPa pressure level at 0 h (UTC). The 1000 hPa pressure level air temperature represents the atmospheric temperature at a specific vertical elevation above the Earth's surface.

To identify extreme temperature events, we focus on abrupt daily temperature changes rather than long-term anomalies. For each grid point, we first remove the mean seasonal cycle from the daily 1000 hPa temperature time series (1979–2021) and normalize by the corresponding seasonal standard deviation, isolating short-term fluctuations from persistent climate trends. Specifically, given a temperature record $\tilde{T}^y(d)$, where y denotes the year and d represents the day of the year (1–365), the filtered record is defined as

$$T^y(d) = \frac{\tilde{T}^y(d) - \mathrm{mean}(\tilde{T}(d))}{\mathrm{std}(\tilde{T}(d))}, \tag{1}$$

where "mean" and "std" denote the long-term mean temperature and standard deviation, respectively, for a specific day d across all years.

We define day-to-day air temperature differences as the current day's air temperature minus the previous day's at each grid from 1979 to 2021. To ensure consistency in the calendar year's duration and simplify the analysis, we excluded leap days. For each of the 6570 grids, we obtained a time series with a length of 15 694. Based on these, positive changes (extremely warm) are defined as daily temperature increases exceeding the 97.5th percentile of the normalized daily differences, while negative changes (extremely cold) are those below the 2.5th percentile—a threshold chosen to capture the top and bottom 2.5% of rare, significant changes, consistent with a 95% confidence interval in statistical hypothesis testing. Consecutive days exceeding these thresholds are aggregated into a single event to avoid counting short-term fluctuations as independent events, particularly relevant for land surfaces where rapid heating/cooling often leads to clustered extreme changes. This definition emphasizes sudden temperature shifts, which are critical for triggering immediate weather impacts and atmospheric wave propagation, differing from conventional definitions of heatwaves/cold spells that focus on sustained temperature deviations from the mean.

B. Finite-size analysis of the climate network

It is worth noting that these nodes do not uniformly cover the entire globe due to the Earth's ellipsoidal shape. To address this non-uniformity, we employ a procedure developed by us.[12] We define the resolution (in degrees latitude) at the equator as r_0 and compute the number of nodes $n_0 = 360/r_0$. Subsequently, the number of nodes at latitude mr_0 is given by $n_m = n_0 \cos(mr_0)$, where $m \in [-90/r_0, 90/r_0]$. The total number of nodes is then calculated as $N' = \sum_{m=0}^{m=90/r_0} (2n_m - n_0)$. Here, we set r_0 to 2.5°, resulting in $N' = 6570$.

C. Synchronization of extreme events

The event synchronization (ES) algorithm operates as follows. Given a percentile threshold p, we denote the set of events above p at grid cell i as $\left\{{}^{p}e_i^{\mu}\right\}_{\mu=1,\ldots,l_i}$, where l_i represents the total number of events at grid cell i. Consecutive events occurring on the same day are counted as a single event. For each pair of grid cells (i,j), ES calculates the count of pairs of uniquely associable events. To ensure uniqueness, we impose the condition that the absolute value of the temporal delay between any two synchronous events μ and ν, denoted as $t_{i,j}^{\mu,\nu} := {}^{p}e_i^{\mu} - {}^{p}e_j^{\nu}$, must be smaller than $\tau_{i,j}^{\mu,\nu} := \frac{\min\left\{t_{i,i}^{\mu,\mu-1}, t_{i,i}^{\mu+1,\mu}, t_{j,j}^{\nu,\nu-1}, t_{j,j}^{\nu+1,\nu}\right\}}{2}$. We set a maximum temporal delay of $\tau_{\max} = 30$ days between events at different locations. Thus, ES for the pair of locations (i,j) is defined as the number of event pairs (μ,ν) that satisfy these conditions,

$$\mathrm{ES}_{ij} := \left\| \left\{ (\mu,\nu) : \left| t_{i,j}^{\mu,\nu} \right| < \tau_{i,j}^{\mu,\nu} \wedge \left| t_{i,j}^{\mu,\nu} \right| \le \tau_{\max} \right\} \right\|. \tag{2}$$

Here, $|a|$ represents the absolute value of a scalar quantity a, and $\|M\|$ denotes the cardinality of a set M. This surrogate model preserves the total number of extreme events in each time series while randomizing their timing, thereby enabling rigorous significance testing.[6]

D. Directional synchronization of extreme events

One key advantage of the ES measure is its ability to incorporate a dynamic delay $\tau_{i,j}^{\mu,\nu}$ within the range $\tau_{i,j}^{\mu,\nu}$, unlike the fixed delay used in traditional lead–lag correlation analyses. Additionally, an adaptation of this measure allows us to pinpoint the exact times when extreme-event synchronization between two regions of interest is high, while maintaining the temporal sequence. For two sets of time series, A and B, associated with two different regions, we define

$$\mathrm{ES}_{A\to B}^{\mu} := \left\| \left\{ (i,j) \in A \times B : -\tau_{i,j}^{\mu,\nu} < t_{i,j}^{\mu,\nu} \le 0 \wedge \left| t_{i,j}^{\mu,\nu} \right| \le \tau_{\max} \right\} \right\| \tag{3}$$

and

$$\mathrm{ES}_{B\to A}^{\nu} := \left\| \left\{ (i,j) \in A \times B : 0 \le t_{i,j}^{\mu,\nu} < \tau_{i,j}^{\mu,\nu} \wedge \left| t_{i,j}^{\mu,\nu} \right| \le \tau_{\max} \right\} \right\|. \tag{4}$$

Here, $A \times B$ represents the Cartesian product of sets A and B, which includes all possible pairs (i,j) such that $i \in A$ and $j \in B$.

Therefore, $ES_{A\to B}^{\mu}(ES_{B\to A}^{\nu})$ can be interpreted as a time series that indicates, for each time step, the number of events in region A (or B) that have a subsequent, uniquely corresponding event in region B (or A).

E. Significance tests

The significance of event synchronization and network construction is determined as follows. To assess the statistical significance of each observed ES_{ij} value, a null-model distribution is generated through numerical computations. This involves calculating ES for 2000 pairs of surrogate event series, where the event numbers l_i and l_j are randomly and uniformly distributed. For each pair (l_i, l_j), the 99.5th percentile of the corresponding distribution is identified as the significance threshold. Based on this null model, a network link is established between locations i and j if the value of ES_{ij} surpasses the significance threshold, indicating its significance at a level of 0.005. It is important to note that by incorporating network links based on the statistical significance of ES_{ij}, potential biases arising from different event rates are eliminated.

F. Climate networks

We utilized the ES method to establish CNs encompassing both directed and undirected CN elements. For each pair of nodes, a network link is established if the corresponding synchronization value is statistically significant at $P \le 0.005$.

1. Degree

In the realm of CNs, a node's degree serves as a pivotal metric, representing the number of connections or links it has with other nodes. This metric is fundamental as it not only quantifies a node's connectivity but also provides profound insights into its significance and role within the overall network structure. In the context of our CN, we specifically interpret a node's degree as the number of other grid cells that exhibit event synchrony with a particular grid cell.

2. In-degree and out-degree

In a directed CN, we adopt two distinct yet complementary metrics to comprehensively describe the degree of node i. In-degree (k_i^{in}): the count of incoming edges directed toward node i, signifying the number of grid cells that synchronize events with node i. Out-degree (k_i^{out}): the count of outgoing edges originating from node i, representing the number of grid cells that synchronize events from node i.

The total degree k_i of node i is defined as

$$k_i = k_i^{\mathrm{in}} + k_i^{\mathrm{out}}.$$

This combined measure captures the overall connectivity strength of the node, regardless of directional bias.

3. Divergence

To characterize directional imbalances in node influence, we introduce the *divergence* metric,

$$D_i = k_i^{\text{out}} - k_i^{\text{in}}.$$

- $D_i > 0$ indicates the net outgoing influence (source node).
- $D_i < 0$ indicates the net incoming influence (sink node).
- $D_i = 0$ indicates the balanced influence (neutral node).

Divergence quantifies the asymmetric role of nodes in propagating extreme-event synchronizations, highlighting regions with disproportionate influence over global teleconnections.

4. Link distance distribution

The link distance distribution is defined as the probability density function (PDF) of Euclidean distances between all pairs of connected nodes in the network.

G. Bias correction method

As elaborated in the main text, outcomes from data-driven interdependency analyses—especially those related to link configurations within functional networks—are typically susceptible to biases induced by multiple comparisons. Herein, we introduce an alternative method to rectify such biases, capitalizing on the spatially embedded nature of the system under scrutiny.[6] The fundamental premise is that links governed by physical mechanisms should manifest spatially coherent patterns, distinguishing them from links originating from random coincidences.

This method utilizes a null model to identify regions forming significant link bundles. To construct a statistical null model for regional link density, we first randomly distribute an equivalent number of links across all grid cells. Subsequently, Gaussian Kernel Density Estimation (KDE) is applied to quantify spatial link density, with the bandwidth determined by Scott's rule and the Haversine metric employed to handle spherical geographic coordinates. By repeating this procedure 1000 times, a null-model distribution is generated for each grid cell, which serves as the baseline for identifying significant link bundles. Specifically, any grid cell where the observed regional link density exceeds the 99.9th percentile of the null-model distribution (i.e., $P < 0.001$) is classified as part of a significant link bundle.

ACKNOWLEDGMENTS

This work was supported by the National Natural Science Foundation of China (NNSFC) (Grant Nos. 42450183, 12275020, 12135003, 12205025, and 42461144209) and the Ministry of Science and Technology of China (No. 2023YFE0109000). J.F. was supported by the Fundamental Research Funds for the Central Universities.

AUTHOR DECLARATIONS

Conflict of Interest

The authors have no conflicts to disclose.

Author Contributions

Yuhao Feng: Software (equal); Visualization (equal); Writing – original draft (equal). **Jun Meng:** Conceptualization (equal); Data curation (equal); Formal analysis (equal); Funding acquisition (equal); Investigation (equal); Methodology (equal); Project administration (equal); Resources (equal); Software (equal); Supervision (equal); Validation (equal); Visualization (equal); Writing – original draft (equal); Writing – review & editing (equal). **Jingfang Fan:** Conceptualization (equal); Formal analysis (equal); Funding acquisition (equal); Investigation (equal); Methodology (equal); Project administration (equal); Resources (equal); Software (equal); Supervision (equal); Validation (equal); Visualization (equal); Writing – original draft (equal); Writing – review & editing (equal).

DATA AVAILABILITY

All data used in this study are publicly available. The Python codes used for the analysis are available on GitHub (https://github.com/AaronFeng29/tas_ere_tele).

REFERENCES

[1] J. Tollefson, "Earth is warmer than it's been in 125,000 years, says landmark climate report," Nature **596**(7871), 171–172 (2021).
[2] A. Morit, "Extreme heatwaves: Surprising lessons from the record warmth," Nature **608**(7923), 464–465 (2022).
[3] P. Kumar, "Climate change and cities: Challenges ahead," Front. Sustain. Cities **3** (2021).
[4] K. Abbass, M. Z. Qasim, H. Song, M. Murshed, H. Mahmood, and I. Younis, "A review of the global climate change impacts, adaptation, and sustainable mitigation measures," Environ. Sci. Pollut. Res. **29**, 42539–42559 (2022).
[5] W. K. Lau and K.-M. Kim, "The 2010 Pakistan flood and Russian heat wave: Teleconnection of hydrometeorological extremes," J. Hydrometeorol. **13**, 392–403 (2012).
[6] N. Boers, B. Goswami, A. Rheinwalt, B. Bookhagen, B. Hoskins, and J. Kurths, "Complex networks reveal global pattern of extreme-rainfall teleconnections," Nature **566**, 373–377 (2019).
[7] G. T. Walker, "Correlations in seasonal variations of weather—A further study of world weather," Monthly Weather Rev. **53**(6), 252–254 (1925).
[8] H. A. Bridgman and J. E. Oliver, *The Global Climate System: Patterns, Processes, and Teleconnections* (Cambridge University Press, 2014).
[9] Z. Liu and M. Alexander, "Atmospheric bridge, oceanic tunnel, and global climatic teleconnections," Rev. Geophys. **45**(2), RG2005, https://doi.org/10.1029/2005RG000172 (2007).
[10] H. Tu, S. Wang, J. Meng, Y. Zhang, X. Chen, D. Chen, and J. Fan, "Eigen microstate analysis unveils climate dynamics," Sci. China Phys. Mech. Astron. **68**, 240511 (2025).
[11] J. Fan, J. Meng, J. Ludescher, X. Chen, Y. Ashkenazy, J. Kurths, S. Havlin, and H. J. Schellnhuber, "Statistical physics approaches to the complex earth system," Phys. Rep. **896**, 1–84 (2021).
[12] J. Meng, J. Fan, Y. Ashkenazy, and S. Havlin, "Percolation framework to describe El Niño conditions," Chaos **27**, 035807 (2017).
[13] J. Meng, J. Fan, Y. Ashkenazy, A. Bunde, and S. Havlin, "Forecasting the magnitude and onset of El Niño based on climate network," New J. Phys. **20**, 043036 (2018).
[14] J. Fan, J. Meng, Y. Ashkenazy, S. Havlin, and H. J. Schellnhuber, "Network analysis reveals strongly localized impacts of El Niño," Proc. Natl. Acad. Sci. U.S.A. **114**, 7543–7548 (2017).
[15] N. Boers, B. Bookhagen, H. M. Barbosa, N. Marwan, J. Kurths, and J. Marengo, "Prediction of extreme floods in the eastern Central Andes based on a complex networks approach," Nat. Commun. **5**, 5199 (2014).

[16] N. Boers, R. V. Donner, B. Bookhagen, and J. Kurths, "Complex network analysis helps to identify impacts of the El Niño Southern Oscillation on moisture divergence in South America," Clim. Dyn. **45**, 619–632 (2015).
[17] Q. Y. Feng and H. Dijkstra, "Are North Atlantic multidecadal SST anomalies westward propagating? Geophys. Res. Lett. **41**, 541–546, https://doi.org/10.1002/2013GL058687 (2014).
[18] H. Hersbach, B. Bell, P. Berrisford, S. Hirahara, A. Horányi, J. Muñoz-Sabater, J. Nicolas, C. Peubey, R. Radu, D. Schepers *et al.*, "The ERA5 global reanalysis," Q. J. R. Meteorol. Soc. **146**, 1999–2049 (2020).
[19] B. Harvey, L. Shaffrey, and T. Woollings, "Equator-to-pole temperature differences and the extra-tropical storm track responses of the CMIP5 climate models," Clim. Dyn. **43**, 1171–1182 (2014).
[20] S. E. Perkins-Kirkpatrick and P. B. Gibson, "Changes in regional heatwave characteristics as a function of increasing global temperature," Sci. Rep. **7**, 12256 (2017).
[21] E. Rousi, K. Kornhuber, G. Beobide-Arsuaga, F. Luo, and D. Coumou, "Accelerated western European heatwave trends linked to more-persistent double jets over Eurasia," Nat. Commun. **13**, 3851 (2022).
[22] D. Sornette and G. Ouillon, "Dragon-kings: Mechanisms, statistical methods and empirical evidence," Eur. Phys. J. Spec. Top. **205**, 1–26 (2012).
[23] M. Sachs, M. Yoder, D. Turcotte, J. Rundle, and B. Malamud, "Black swans, power laws, and dragon-kings: Earthquakes, volcanic eruptions, landslides, wildfires, floods, and SOC models," Eur. Phys. J. Spec. Top. **205**, 167–182 (2012).
[24] S. Wang, J. Meng, and J. Fan, "Exploring the intensity, distribution and evolution of teleconnections using climate network analysis," Chaos **33**, 103127 (2023).
[25] Y. Zhang, J. Fan, X. Chen, Y. Ashkenazy, and S. Havlin, "Significant impact of Rossby waves on air pollution detected by network analysis," Geophys. Res. Lett. **46**, 12476–12485, https://doi.org/10.1029/2019GL084649 (2019).
[26] W. Cai, M. Lengaigne, S. Borlace, M. Collins, T. Cowan, M. J. McPhaden, A. Timmermann, S. Power, J. Brown, C. Menkes *et al.*, "More extreme swings of the south pacific convergence zone due to greenhouse warming," Nature **488**, 365–369 (2012).
[27] R. Goyal, A. Sen Gupta, M. Jucker, and M. H. England, "Historical and projected changes in the southern hemisphere surface westerlies," Geophys. Res. Lett. **48**, e2020GL090849, https://doi.org/10.1029/2020GL090849 (2021).
[28] A. A. Tsonis and K. L. Swanson, "Topology and predictability of El Nino and La Nina networks," Phys. Rev. Lett. **100**, 228502 (2008).
[29] J. F. Donges, Y. Zou, N. Marwan, and J. Kurths, "Complex networks in climate dynamics: Comparing linear and nonlinear network construction methods," Eur. Phys. J. Spec. Top. **174**, 157–179 (2009).
[30] T. M. Lenton, H. Held, E. Kriegler, J. W. Hall, W. Lucht, S. Rahmstorf, and H. J. Schellnhuber, "Tipping elements in the Earth's climate system," Proc. Natl. Acad. Sci. U.S.A. **105**, 1786–1793 (2008).
[31] T. M. Lenton, J. Rockström, O. Gaffney, S. Rahmstorf, K. Richardson, W. Steffen, and H. J. Schellnhuber, "Climate tipping points—Too risky to bet against," Nature **575**, 592–595 (2019).
[32] C. A. Nobre, G. Sampaio, L. S. Borma, J. C. Castilla-Rubio, J. S. Silva, and M. Cardoso, "Land-use and climate change risks in the Amazon and the need of a novel sustainable development paradigm," Proc. Natl. Acad. Sci. U.S.A. **113**, 10759–10768 (2016).